UNIVERSITY OF CALIFORNIA, SAN DIEGO

Suppressible Pinning of Abrikosov Vortices: Effects of Magnetic Vortex Arrays on Thin Superconducting Films

A Thesis submitted in partial satisfaction of the requirements
for the degree Master of Science

in

Physics
with Specialization in Materials Physics

by

Kevin Daniel Smith

Committee in Charge:

Professor Ivan K. Schuller, Chair
Professor Massimiliano Di Ventra
Professor Oleg Shpyrko

2008

The Thesis of Kevin Daniel Smith is approved and it is acceptable in quality and form for production on microfilm:

_____

_____

_____
Chair

University of California, San Diego

2008

TABLE OF CONTENTS

LIST OF FIGURES

LIST OF TABLES

LIST OF GRAPHS

ACKNOWLEDGEMENTS

I would like to acknowledge Professor Ivan Schuller for his support as my adviser and as the chair of my committee. The resources he provided by means of his Mayer Hall laboratory, fellow researchers, and abiding guidance made my entire graduate existence possible.

I would like to acknowledge Dr. Javier Villegas for imparting the constant direction, fellowship, and intimate knowledge essential to this research project. I am fortunate to have co-authored a paper with Dr. Villegas for which he was the primary investigator and author.

The paper has been submitted for publication in Physical Review B, 2008, J.E. Villegas; K.D. Smith; Lei Huang; Yimei Zhu; R. Morales; Ivan K. Schuller, The American Physical Society, 2008. Though not explicitly reprinted in the thesis, the works are analogous and it was regularly and readily consulted.

ABSTRACT OF THE THESIS

Suppressible Pinning of Abrikosov Vortices:
Effects of Magnetic Vortex Arrays on Thin Superconducting Films

by

Kevin Daniel Smith

Master of Science in Physics
with Specialization in Materials Physics

University of California, San Diego, 2008

Professor Ivan K. Schuller, Chair

A thin superconducting/ferromagnetic heterostructure was constructed for which it was found that the collective pinning of Abrikosov vortices can be induced or prevented depending on the ordering of a ferromagnetic dot array. Arrays in the magnetic vortex state will induce flux pinning if uniformly polarized, but a demagnetized, disordered array will not have collective commensurability with the flux lattice. The system also exhibits field-induced superconductivity as a byproduct of the interaction between magnetic vortex stray fields and penetrating flux quanta.

Introduction

Nanostructured hybrid systems comprising superconductors and magnetic elements (S/M systems) have demonstrated an assortment of interesting properties, such as domain-wall superconductivity, proximity effects, improvement of critical current and field thresholds, and Abrikosov vortex pinning in type-II superconductors [1-16]. S/M systems have been shown to carry overcritical currents in the Meissner state when a self-induced or applied magnetic field is shielded by an adjoining magnetic component. In the mixed state, the flux quanta lattice can be significantly altered as it interacts with the pinning potentials created by the moments of a ferromagnetic influence[16-18]. The interaction between elastic lattices and pinning potentials is not unique to type-II superconductors; it is witnessed in a variety of physical systems, e.g. repulsive colloidal particles and Bose-Einstein condensates in optical lattices, and charge density waves in solids [19-21]. The properties of all these systems are strongly affected by this interaction, and ultimately by the geometry and degree of order of the pinning substrate [11,22]. This is dramatically illustrated through the use of artificial pinning potentials, where commensurability with periodic and quasiperiodic potentials induces collective and/or local pinning and controls lattice correlation lengths [12,13]. Such an artificial pinning system is the basis of this study.

Ordered arrays of magnetic nanodots are commonly used to create pinning potentials for the flux-lattice in superconducting thin films [6-8, 10-12]. Dots of various diameters and arrays of various spacing have been used in many studies to see what effect the geometry of the pinning substrate has on the superconductor. Not until

recently, however, were superconductors studied for which the ground state of the dot array is in the non-uniform "magnetic vortex" state (not to be confused with the mixed Abrikosov vortex state of a type-II superconductor) [23-28]. Dots in the vortex state are intriguing for two reasons. First, the subtle differences between the multidomain state and vortex state magnetizations have been shown to produce significant differences in the behavior of the superconductor. Second, the magnetic state of the dots can be easily controlled with applied fields comparable to and even less than the superconducting critical fields, a unique feature that adds a finer level of control in the study of Abrikosov lattice dynamics in S/M heterostructures.

S/M systems utilizing magnetic vortex arrays have exhibited novel hybridized properties, as the characteristics of the ferromagnets are exemplified in the transport properties of the superconductor through changes in the *ordering* of the array. With a superconducting thin film in-plane with an applied field, magnetic vortices can induce very unusual transport effects including a giant hysteretic magnetoresistance (10^5 %) [28]. Below superconducting critical temperatures, bi-stable magnetotransport develops and can switch between a reversible low-resistance state and an irreversible high-resistance state. It is simply the magnetic ordering of the vortices in the array that determines the state of the superconductor. The disordered virgin array allows the film to remain superconducting at low fields, while the ordered saturated array inhibits the film from returning to its fully superconducting state. It was concluded that these effects can be attributed to interaction of the superconductor with the *out-of-plane* stray-field of the magnetic vortex. The goal of the current study is to provide an extension to this research by further isolating and analyzing this interaction.

Like the system described above to induce bi-stable superconductivity in thin films, the current setup consists of a magnetic dot array in the vortex state and a superconducting thin film. However, the dots are now isolated on top of (as opposed to within or under) the superconductor, and the geometry of the arrays have been altered such that Abrikosov vortex pinning is readily induced with the application of an out-of-plane external field. The system is designed to toggle the collective pinning of flux quanta by switching *on* and *off* the magnetic ordering of the pinning substrate. If the array is "magnetized" (all the vortex polarities aligned), a periodic pinning potential is obtained, which causes collective pinning and induces a square symmetry order in the flux-lattice. If the array is "demagnetized" (balanced distribution of vortex polarities), a disordered pinning potential is obtained, and no commensurability develops between the flux-lattice and the dot array. In addition to these effects, the system exhibits field-induced superconductivity, which originates here from the annihilation of dipole-induced flux quanta when the field is applied. Much of the behavior of this system is previously unseen and will be discussed later in the report.

Theory

Type-II superconductivity is an area of research receiving much interest recently, noted by the 2003 Nobel Prize awarded to A.Abrikosov for his pioneering work in the field. At certain temperatures and fields these superconductors experience a mixed (vortex) state, in which magnetic flux is able to penetrate the material without globally destroying its superconductivity. As with all superconductors, below a critical temperature and field the material is a perfect diamagnet (susceptibility = -1), rejecting all magnetic flux. The superconductor remains in this state until the external applied field reaches a lower critical value, H_{c1}, when magnetic flux quanta begin to pass through the material. Within these columns of flux quanta (Abrikosov vortices), the magnetic field inhibits Cooper pairing, and the material is in the normal state.

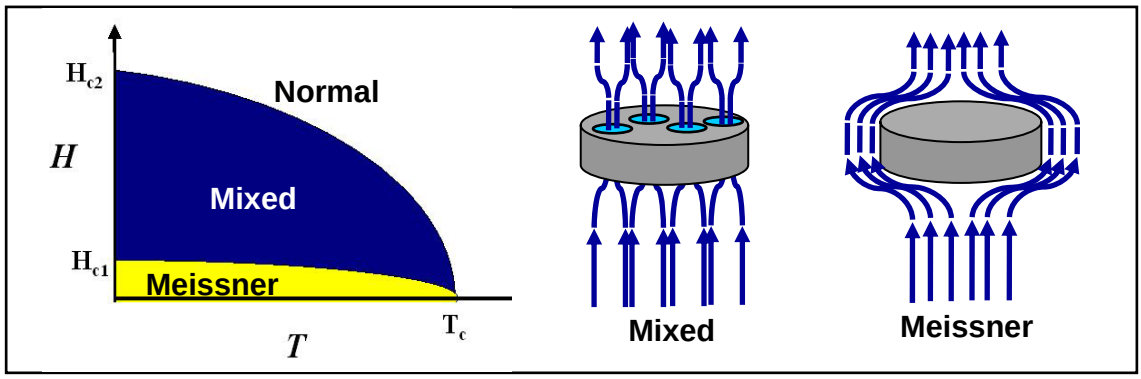

Figure 1: States of a type-II superconductor as they relate to temperature and field.

The vortices have core radii of an approximate length ξ, the superconducting coherence length of the material. Screening the magnetic flux vortex from the rest of the bulk is a circulating supercurrent around the normal core of the vortex. This supercurrent decays exponentially to zero over the distance λ, the London penetration depth of the material (Thus, to sustain superconductivity throughout the material while in the mixed state,

type-II superconductors have characteristic penetration depths greater than their coherence lengths: $\lambda / \xi > 1$).

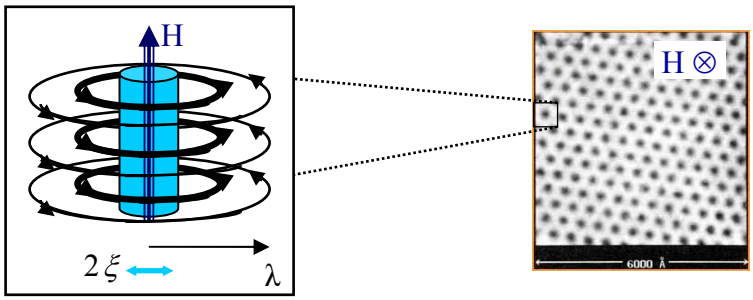

Figure 2: Single Abrikosov vortex in a triangular array of vortices.
H.F. Hess, R.B. Robinson, R.C. Dynes, J.M. Valles,Jr., and J.V Waszczak, Phys. Rev. Lett. ***62****,214 (1989).*

As shown in Figure 2, the circulating supercurrents drive the vortices to repel each other such that, in the absence of disorder, the vortices arrange themselves in a triangular lattice. As the external field is increased, additional flux quanta pierce the material until the vortex cores begin to converge. At this upper critical field, H_{c2}, the normal state of the increasing vortex cores dominate the material, and superconductivity in the bulk is lost.

Applying a current across a type-II superconductor in the mixed state leads to a supplementary effect and research concentration: vortex dynamics. A current density, J, in a magnetic field, B, generates a Lorentz force, $F_l = J \times B$, which acts upon the flux vortices. Above critical field and current densities, this force causes the vortices to move with a velocity, v, in turn producing an electric field in the superconductor, $E = v \times B$. The electric field quells the superconducting state of the material; the current can no longer flow without dissipation, and a voltage appears across the sample. Vortex motion eliminates the ability to maintain superconductivity at high fields and currents. Of great interest, then, is the prevention of Abrikosov vortex motion: pinning.

Stationary vortices do not produce an electric field in the bulk material, and current can percolate dissipation free between the pinning sites. For a vortex to be held still in the midst of a current density, its pinning force, F_p, has to be greater than the electromagnetic Lorentz force acting on it. Pinning forces can be created by various mechanisms of disorder such as dislocations, interstitials, inhomogeneities, etc., or by an extrinsic influence such as a nearby nanoparticle [10,16-18].

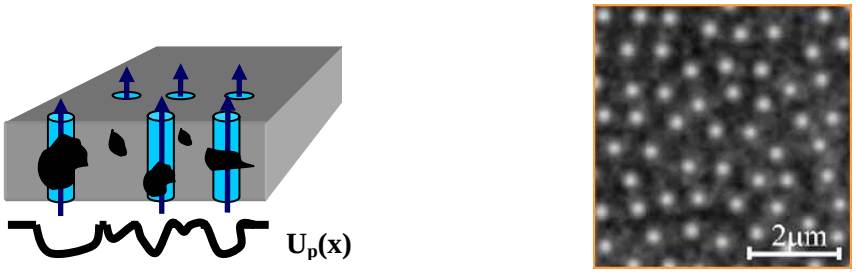

Figure 3: Disordered pinning potential and corresponding vortex pinning, induced by inhomogeneities in the superconductor. *A. Volodin, K. Temst, C. Van Haesendonck, Y. Bruynserede, M.I. Montero, I.K. Schuller, Europhys. Lett.* ***58*** *582 (2002).*

As shown in Figure 3, Nanoparticles on the surface of (or contained within) a type-II superconductor can alter the Bean-Livingston barrier for magnetic flux entry and exit [29], and will therefore induce pinning locations for Abrikosov flux vortices. The particles themselves contribute to "structural pinning" brought on by physical variation and inconsistencies in the bulk [9], but much more intriguing effects can be induced by magnetic natured nanoparticles of varying construction (dots, rings, triangles, etc.). A number of magnetic mechanisms originating from the nanostructures contribute to vortex pinning, including proximity effect, magnetic reversal losses, and stray magnetic field interactions with the flux quanta. If stray field interaction is isolated as the primary

pinning mechanism, it follows that the pinning potential landscape is significantly affected by the magnetic characteristics and state of the nanoparticles.

Ferromagnetic nanodots are useful in studying pinning in thin films, as they are able to retain magnetization even after an applied external field is removed. This allows for the manipulation of the applied external field to be independent from the "permanent" saturated magnetic state of the array. Asymmetric (field polarity dependent) pinning and pinning potentials of tunable strength have been observed using ordered arrays of these magnetic nanodots. In these arrays, the nanodots possess essentially identical magnetic multidomain states and equal remanent magnetizations M. Consequently, the interactions between a flux quantum and every magnetic particle in the array are essentially identical across the sample, and changes in M do not affect the ordering of the pinning potential, which is fixed by the array geometry.

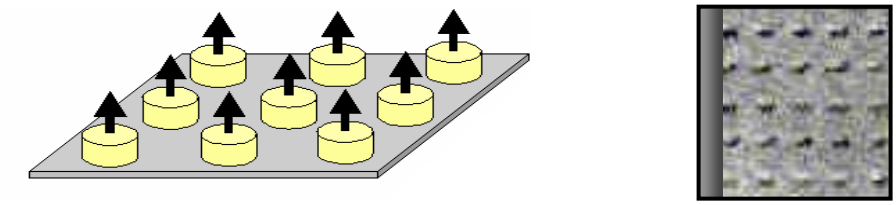

Figure 4: An ordered array of ferromagnetic dots induces an ordered flux quanta lattice in the superconductor. *K. Harada, O. Kamimura, H. Kasai, T. Matsuda, A. Tonomura, V.V. Moshchalkov, Science* ***274****, 5290 (1996).*

Recently, advances in nanofabrication techniques have permitted the exploration of S/M hybrid systems containing ordered arrays of magnetic dots in the "magnetic vortex" state. In such systems, magnetic reversal takes place via the nucleation, displacement, and annihilation of magnetic vortices, a very dynamic process as opposed to the fixed geometric effect of previous studies. Many sub-micron disk-shaped

ferromagnets (dots) have a magnetic vortex ground state, as the geometry of the dot is such that its minimal energy configuration is magnetically non-uniform. The dot possesses a magnetization that curls in-plane (chirality) around a central core, in which the magnetization points out-of-plane (polarity).

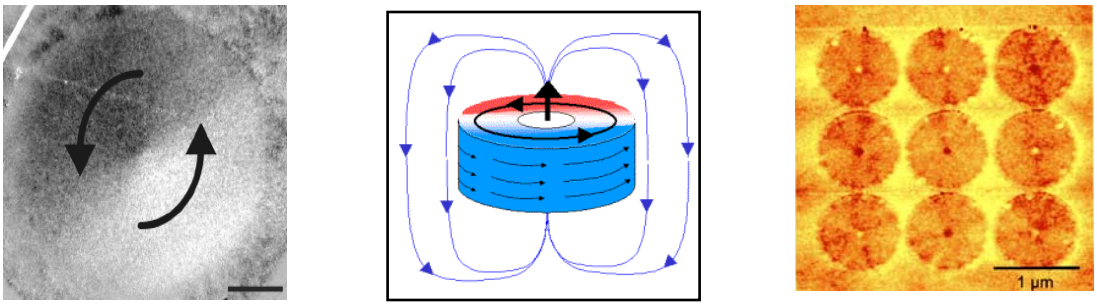

Figure 5: A single dot and an array of dots in the magnetic vortex state.
*T. Shinjo, T. Okuno, R. Hassdorf, K. Shigeto, T. Ono, Science **11,** 289 (2000).*
*T. Taniuchi, M. Oshima, H. Akinaga, K. Ono, J. Appl. Phys. **97**, 10J904 (2005).*

The transition from uniform to vortex magnetization is easily observed using the Magneto-optic Kerr effect (MOKE). Moreover, magnetic force microscopy can provide a visual representation of the vortex chirality and polarity [30,31]. An array of dots in the magnetic vortex state can be magnetized by having all the dots polarized in the same direction, or demagnetized by having an equal number of its dots polarized "up" as are polarized "down." Ideally, the distribution of polarities will be balanced and random, differing from previously studied arrays in which demagnetization refers to the state of each individual dot [32,33].

Methodology

Before one can obtain data of any significant use, quality samples must be fabricated by paying careful attention to proper methods and procedures. For the S/M heterostructures used in this study, their production consists of more than 20 individual steps spread over 3 fundamental processes: thin-film deposition, electron beam lithography, and optical lithography. All lithography processes described here were conducted in an ultraviolet free clean room, and intermediately stored in vacuum to control oxidation.

The thin films used for transport measurements were created by evaporating a layer of aluminum on top of 1 cm × 1 cm cut sapphire substrates. These Al films were grown in a custom high voltage e-beam evaporation system to thicknesses ranging from 13 – 33 nm, then exposed to the air to obtain a ~3nm thick AlO_x capping layer. This layer of oxide serves the purpose of separating the dot array from the superconducting film. To verify the thickness of the film and calibration of the deposition, a deposited sample was analyzed in an X-ray diffraction system.

Graph 1: θ - 2θ X-Ray Diffraction analysis of a 10 second deposition.

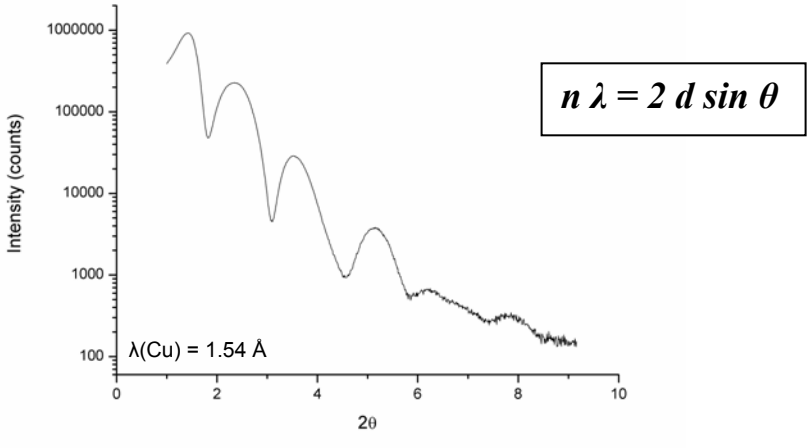

The measurements were predicted by prior calibration, with 10 and 25 second depositions providing thicknesses of 13 and 33 nm, respectively.

After oxidation, the films were prepared for patterned exposure in a scanning electron microscope (SEM). A 400NM layer of poly(methyl methacrylate) (PMMA) positive resist was spin-coated on top of the Al/AlO_x layer at 6000RPM for 1 minute, and then baked at 155°C for 2 hours. Exposure doses ranged from 40 – 100 $\mu C/cm^2$ for patterns of dot arrays defined on a square area measuring 50 μm × 50 μm. Array patterns varied in interdot distances from 0.6 – 1 μm, and in dot diameters from 430 – 490 nm. After e-beam exposure, the samples underwent a controlled developing process at 16° C. They were immersed in a 3:1 developer/ethanol solution for 40 seconds, then in a 1:3 MIBK/IPA rinse solution for 15 seconds. With the array patterns now etched into the resist, the samples were ready for the deposition of the ferromagnetic layer which constitutes the dots themselves. A 40 nm layer of cobalt was sputtered on top of the sample in an UHV Microscience IBEX-2000 DC Sputtering Chanmber, then a 2nm cap layer of gold was sputtered to prevent Co oxidation. To remove the layer of resist and obtain the final structure, the samples underwent a simple lift-off immersion in acetone. The samples were then returned to the SEM for image verification. With the sapphire – aluminum – alumina – cobalt – gold heterostructure complete, the photolithographic process necessary for transport measurements can begin.

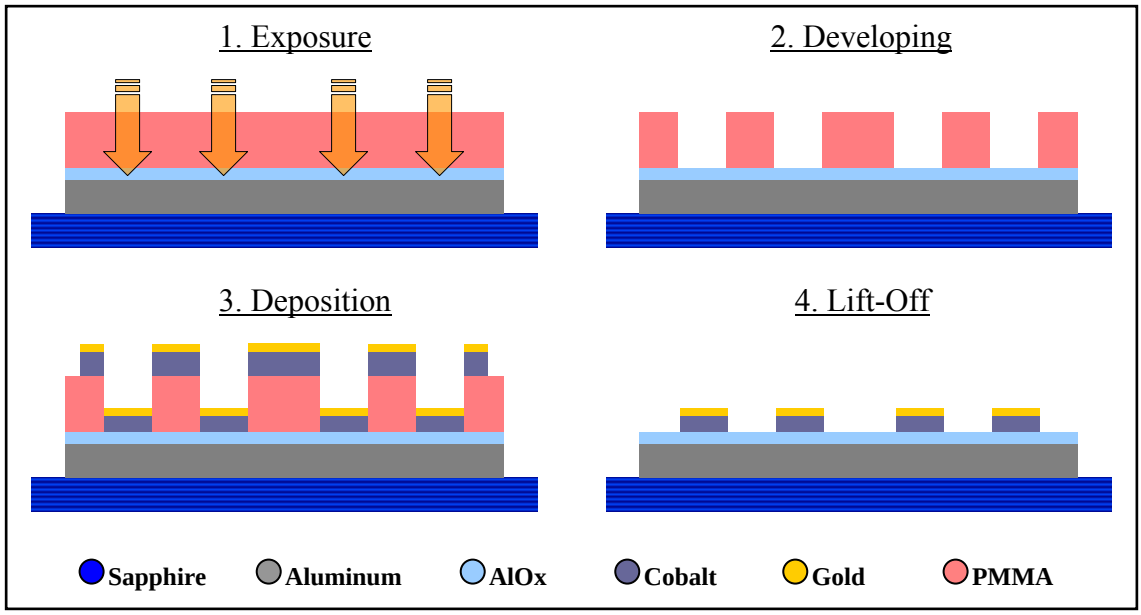

Figure 6: Sample fabrication process. (not to scale)

The samples were spin-coated with 1.6 μm Shipley MicroPosit S1818 positive photoresist at 5000RPM for 1 minute, and then baked at 115° C for 1 minute. A photomask of a 40 μm × 40 μm standard four-probe bridge was aligned directly on top of the 50 μm × 50 μm dot array using a Karl Suss MJB3 Mask Aligner, and the samples were subjected to an ultraviolet exposure lasting 40 seconds. A 1:1 MicroDev/H_2O solution was used to remove the exposed resist, leaving the resist in the pattern of the bridge. Samples were placed in a Reactive Ion Etching unit (RIE), in which all the material not protected by the photoresist is etched away by an Argon plasma. The photoresist is easily removed by immersing the substrate in acetone, leaving a 40 μm × 40 μm Co dot array on top of an Al thin film layer which also contains the bridge and its eight contact points.

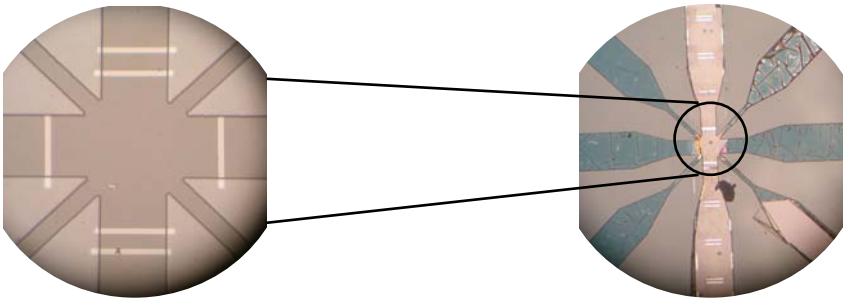

Figure 7: Intermediate steps of the photolithography process.
Picture on the left shows the dot array after the resist pattern has been set.
Picture on the right shows the eight contact bridge after RIE and a partial acetone immersion.

To verify the vortex state of the Co dots, two methods of characterization were used. Using a MOKE (Janis SuperOptiMag Cryostat), pre-photolithographed dot arrays had their magnetization monitored as fields were swept. Samples were then examined using Lorentz microscopy, providing visual representation of the vortex polarity of the dots in both the magnetized and demagnetized conditions.

Magnetotransport measurements were conducted in a liquid He cryostat capable of maintaining temperatures as low as 1.2 K. The sample plane (with injected currents and measured voltages residing in this plane), was oriented normal to the applied magnetic field. A nanovoltmeter was used to monitor the resistance across the sample as fields were swept at different current levels and temperatures. From the cryostat data alone, field-, current-, and temperature-dependencies of each sample could all be found.

The following page lists and shows the fabricated samples that underwent magnetotransport measurements.

Table 1: Sample characteristics.

Sample ID	Film Thickness	Array Spacing	Dot dia.
ALk1	33 nm	600 x 600 nm	~ 413 nm
AL25k	33 nm	1000 x 1000 nm	~ 427 nm
AL10k3	13 nm	600 x 600 nm	~ 499 nm
AL10k4	13 nm	1000 x 1000 nm	~ 484 nm

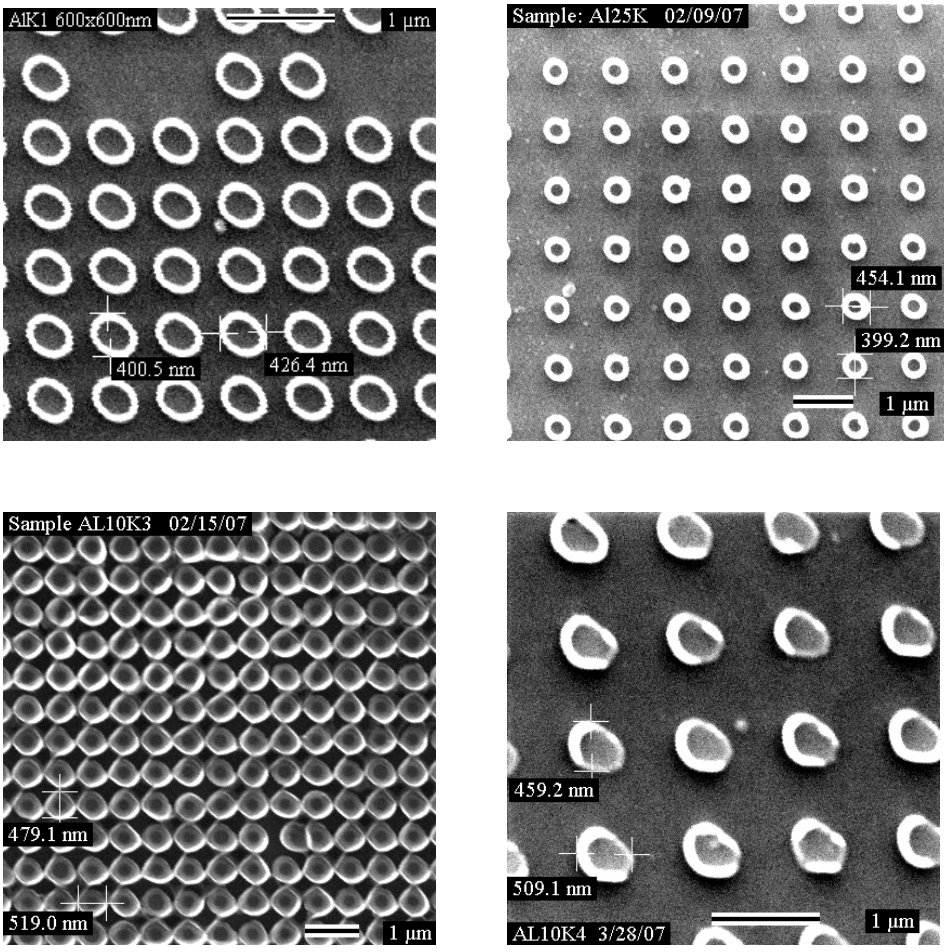

Figure 8: SEM images of the four tested samples at various magnifications.

Results

The first experimental objective was to characterize the aluminum films by their superconducting dependencies on temperature and field. With no applied field, each film was brought from room temperature to 1.2 K while having its resistance, R, monitored. Transitions from the normal state to the superconducting state occurred at T_c = 1.95 – 1.98 K for the 13 nm samples, and T_c = 1.63 – 1.66 K for the 33 nm samples (T_c is defined at the point where R = .9 ρ, where $\rho = R_{normal}$). Graph 2 shows the superconducting transition for sample AL10k3, and is typical of all the samples.

Graph 2: Temperature induced superconducting transition of sample AL10k3. Here, a sharp drop in resistance is observed at 1.9 K.

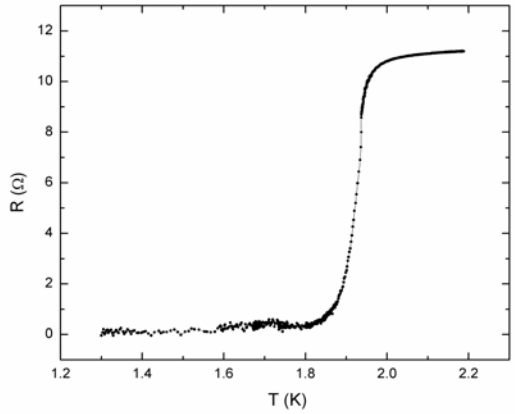

Knowing T_c and the residual normal state resistance, ρ, in Ohms, of a dirty superconductor allows for the calculation of the London penetration depth [34]:

$$\lambda_0 = 1.29 \times 10^{-2} \, (\rho / T_c)^{1/2}$$

Penetration depths were found to be $\lambda(0) \approx 220 – 350$ nm.

Each film was brought from an applied saturation field H = 20 kOe to zero field, at constant temperature below T_c, while having its resistance monitored. The upper critical

field, H_{c2}, was recorded for R = .9 ρ, Knowing H_{c2} allows for the calculation of coherence length using the Ginzburg-Landau dependence:

$$\xi(T)^2 = \xi_0^2 / (1 - T / T_c) \qquad H_{c2} = \varphi_0 / 2\pi\,\xi(T)^2$$

Coherence lengths were found to be $\xi(0) \approx 40 - 50$ nm. Therefore, the Al films studied here are verified type-II superconductors, as $\kappa(0) = \lambda(0) / \xi(0) \approx 4.5 - 8.5$.

With the analysis of the Al films complete, the second experimental objective was to characterize the dependence of M as a function of field for the cobalt dots. The aspect ratio of the dots was chosen so that their magnetic ground-state is a "magnetic vortex," but this needed to be verified in the MOKE. Graph 3 shows the in-plane hysteresis loop of an array of cobalt dots (40nm thick, 450nm diameter, 600nm square lattice spacing) on top of a gold base layer (33 nm).

Graph 3: MOKE hysteresis loop of cobalt dots on gold.

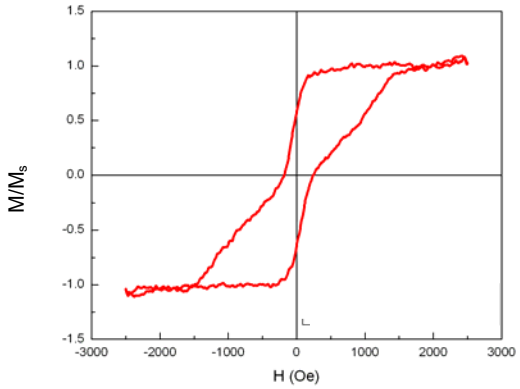

The pronounced pinching in the middle of the loop is characteristic of magnetic reversal via the nucleation, displacement, and annihilation of magnetic vortices[23,27]. The following cartoon depicts this process from negative to positive saturation (- red, + blue). The flux-closure nature of the vortex state causes the stray magnetic field of each dot to effectively act as a dipole; this is illustrated in the inset.

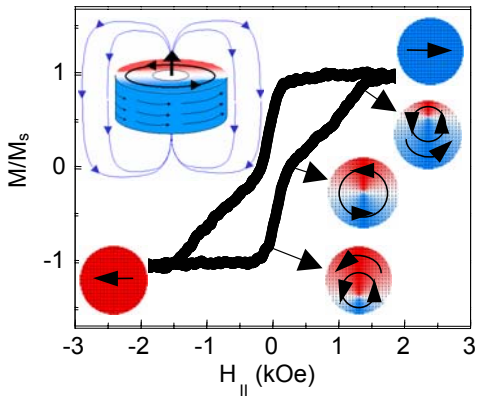

Figure 9: Vortex nucleation, displacement, and annihilation in a sweeping magnetic field.

Now that the magnetic state of the dots was verified, their ordering (distribution of polarities) within the array had to be examined. As seen before, after the application and removal of a saturating out-of-plane field, all the magnetic vortices will have the same polarity in the remanent state. However, when the array undergoes an out-of-plane demagnetizing cycle, the distribution of polarities is expected to be balanced in both directions. To check this, samples were sent to Brookhaven National Labs to Yimei Zhu to be analyzed using Lorentz microscopy. This provided a clear visual representation of the dots' vortex magnetization. As is seen in Figure 10, polarities of both directions were obtained.

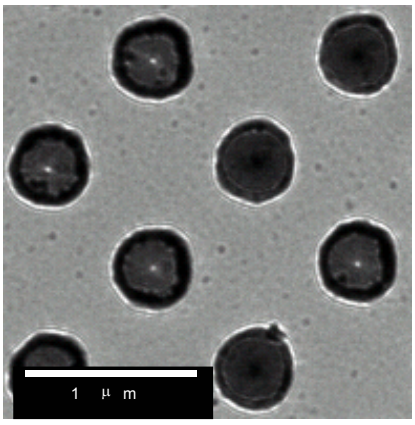

Figure 10: Lorentz image of a demagnetized Cobalt dot array.
White centers indicate vortex polarity out of the page.

This study differs from previous research due to the isolation of the Co arrays from the superconducting Al layer. Placing the array on top of the superconductor with an AlO_x insulating layer reduces contributions from proximity effect, structural corrugations, and interfacial effects on vortex nucleation. This provides assurance that the governing pinning mechanism is the stray field interaction between magnetic vortex cores of the dots and flux quanta in the superconductor.

The two states of magnetoresistance for the 13 nm samples are shown below in Figure 11. A large shift in resistance is observed depending on the magnetic history of the array.

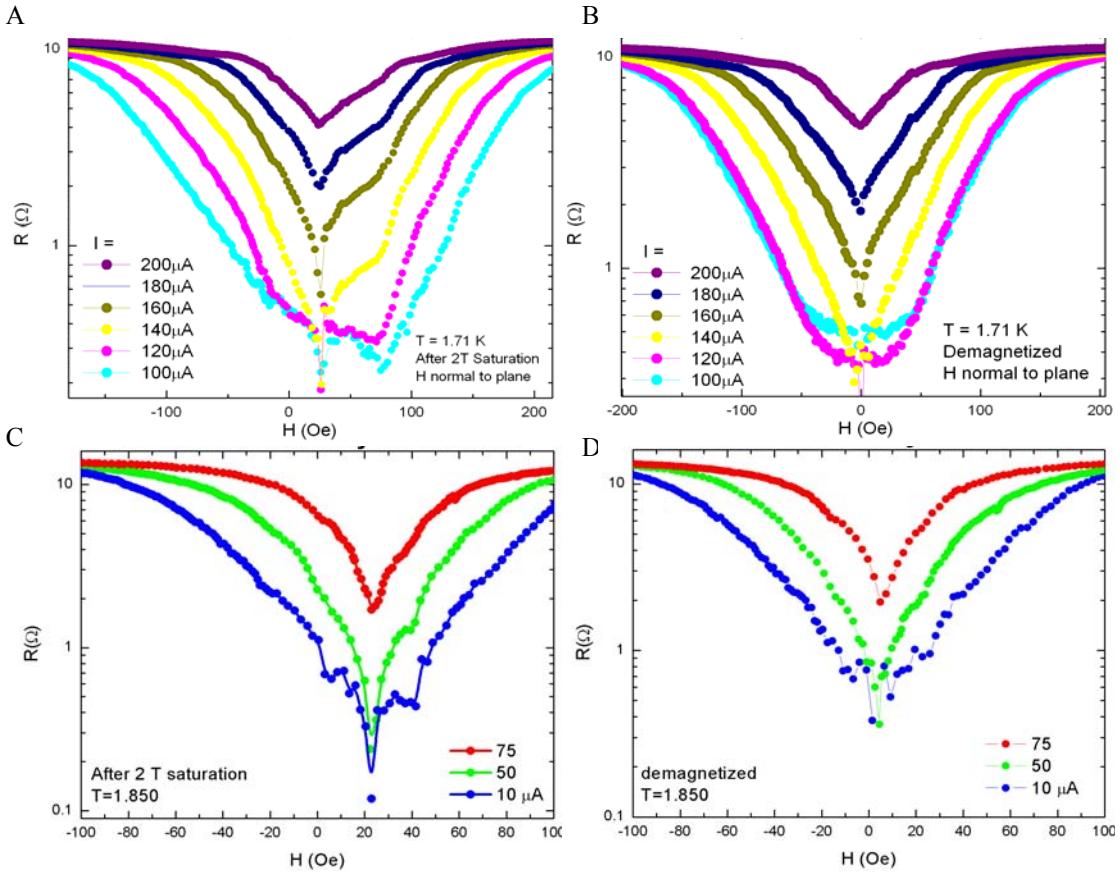

Figure 11: Magnetoresistance for the 13nm samples. A & B (C & D) show magnetized and demagnetized curves for the 600x600 (1000x1000) nm array.

Figure 11 A & C show the magnetoresistance after a field H = 20 kOe, perpendicular to the sample plane, was applied prior to measurements. This field is large enough to saturate the array such that all the vortex cores are aligned in the same direction. This polarity distribution remains unaltered during R(H) measurements since H < 400 Oe, well below the field strength of several kOe needed to reverse the core magnetization. In the magnetized curves, three significant features stand out. First, the absolute minimum of R(H) is not at H = 0, but shifted to a field H_S; this is an effect known as field-induced-superconductivity[35]. This shift corresponds to a magnetic flux $H_S\, a^2 \approx 0.5\, \varphi_0$ per unit cell of the square array ($\varphi_0 = 2.07 \times 10^{-7}$ Mw, the flux quantum). Second, minima appear at $H = H_S + H_1$, with $H_1 = \varphi_0 / a^2 \approx 50$ Oe for sample AL10k3, and ≈ 20 Oe for sample AL10k4. These minima are suppressed at higher currents (and higher temperatures), but they imply there are matching effects between the flux-lattice organization and the square geometry of the magnetic vortex array [6]. Third, the magnetoresistance, R(H), is highly asymmetric. With a positive saturated array, the background resistance is lower for fields $H > H_S$ than for $H < H_S$. Also, the commensurability effects that are so apparent at $H = H_S + H_1$, are much less noticeable at $H = H_S - H_1$.

Figure 11 B & D show the magnetoresistance after an out-of-plane demagnetizing cycle (a series of loops of decreasing amplitude, from H = ± 20 kOe to H = 0) was applied prior to measurements. The magnetic vortex polarities are then balanced for the array as a whole and, just as in the magnetized case, these polarities remain unaltered throughout the R(H) measurements. In the demagnetized curves, the resistance is symmetric about H = 0, and no commensurability effects are observed.

To appreciate these stark contrasts in magnetoresistive behavior, we must closely examine the difference in polarity ordering and how that affects the system as a whole. The net flux through the Al film from a Co dipole is essentially zero, as the positive flux just underneath the dot is equal and opposite to the negative flux returning through the film surrounding the dot. Thus, when flux quanta are induced in the superconductor by a sufficiently strong dipole, positive flux quanta $+\varphi_0$ will be confined just underneath the dot while the same number of negative flux quanta $-\varphi_0$ will be arranged around it (these can be either single quanta or "giant" multiquanta) [36-38]. So, having a square array of positive dipoles, the induced negative flux quanta will arrange themselves to minimize the repulsion energy of the dots, and will occupy the equidistant interdot spaces [36]. Figure 12 illustrates the distribution of flux quanta as they relate to the dipoles as a function of external applied field.

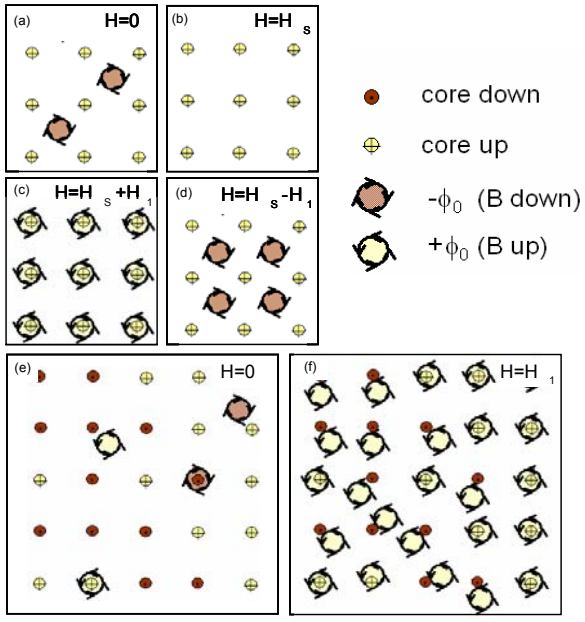

Figure 12: Flux quanta distribution amongst an array of magnetic dipoles, as a function of external applied field

Figure 12 A-D correspond to the array of magnetized Co dots after a large positive saturation field has been applied and removed, so all dipoles are aligned and positively polarized (ordered). When the external field H = 0, the inter-dipole area of the film is penetrated by negative flux quanta, solely stemming from the stray magnetic field of the dots. At this stage, due to these penetrating Abrikosov vortices, the superconductor has a small resistance.

When a positive external field is applied, it induces positive flux quanta in the film, which annihilate the dipole-induced negative flux quanta [36]. When all of the vortices are annihilated, at H_S, the absolute minimum resistance of the superconductor is observed. In this respect, the system exhibits field-induced superconductivity. As the external field is increased further, more positive flux quanta are induced in the film, increasing the resistance until $H = H_S + H_1$, where a second minimum develops. This is due to the ceasing of vortex motion (flux pinning), which occurs at certain matching configurations between the field-induced flux-lattice and the geometry of the dot array.

When a negative external field is applied, it induces negative flux quanta in the film, which compliment the already present negative flux quanta and increase resistance. A shallow minimum is observed at $H = H_S - H_1$, a field strength corresponding to the matching configuration of the lattice. However, as stated before, negative flux pinning in the interstitial sites is much less effective than the positive flux pinning directly underneath the dipoles. This difference in pinning strength is the main contributor to the asymmetry seen in Figure 11 [7,8].

Figure 12 E-F correspond to the array of Co dots after an external demagnetizing cycle was applied and removed. As seen in analogous arrays with large distances between vortex cores, the distribution of polarities within the dot array is both balanced and disordered [24,25]. When the external field H = 0, the minimum of the R(H) curve is observed, indicating little or no commensurability between the superconductor and the ferromagnetic array. This is due to the cancellation of stray fields with neighboring dipoles, and allows for only a very limited number of induced flux quanta (in localized areas that by chance share similarly polarized dipoles). When a positive external field is applied, it induces positive flux quanta, some of which find favorable pinning sites under polarized dipoles while others find interstitial sites preferable. This disordered flux lattice is never pinned collectively, only becoming more crowded with unpinned flux quanta (with an increase in resistance) as the external field is increased [13-15].

Verifying the illustrative representation of the results is a calculation of the field penetration through the superconductive film as it relates to the size of the magnetic vortex cores in the cobalt dots. Experimental magnetization profiles of Co vortex cores have provided the following model [30]:

$$M_{\perp}[r] = M_S\,(\Theta[2 - r] + \Theta[r - 2](R - r)/(R - 2))$$

with R the core radius (in nm), r the distance from the core center, $\Theta[x]$ the Heaviside step function, and M_S = 1.43 kOe the saturation magnetization. From this, the *out-of-plane* component of the induced magnetic field at the Al film plane, $H_{\perp}(r)$, can be found. For R = 40, both $M_{\perp}[r]$ and $H_{\perp}(r)$ are shown below.

Graph 4: The out-of-plane magnetic field profile of a vortex core with radius R = 40nm.
Left: The magnetization profile within the magnetic vortex core.
Right: Flux through the core as a function of core radius.

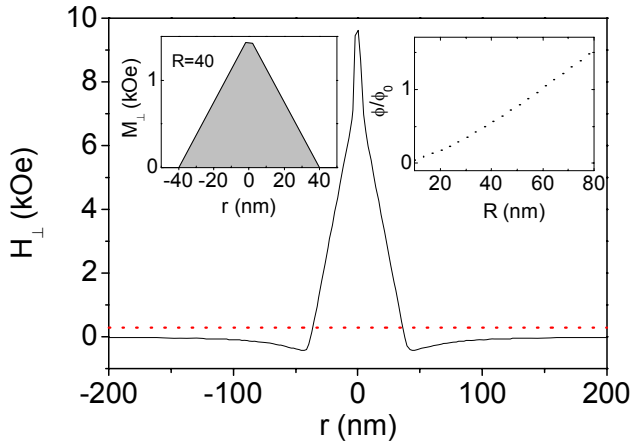

Also plotted above is the flux of this field through the core area, φ, as a function of the core radius R, in units of the flux quantum φ_0. With no external field applied to the magnetized array, the positive flux through the superconductor φ_s^+ beneath each vortex core is equal to the negative flux per unit cell φ_s^- between the cores, but due to screening effects from Meissner currents these values will be less than the total flux through the core itself ($\varphi_s^+ = \varphi_s^- < \varphi$) [37,38]. Using the observed shift Hs in the R(H) curves (for which $H_S a^2 = \varphi_s^+ = \varphi_s^-$) and φ(R), the estimated core radius R > 40 – 60 nm, depending on the sample. Interestingly, for R < 60nm the flux through the superconductor just underneath the vortex core must be less than a single flux quantum, a unique trait attributed to the relative length scales of the vortex core, coherence length, and penetration depth. The field from the cobalt core is concentrated over a distance R that is smaller than both the coherence length $\xi(0.84\ T_c) \approx 100$ nm and penetration depth

$\lambda(0.84\ T_c) \approx 550$ nm, allowing for suppression of superconductivity directly under the dipoles without necessitating the penetration of flux quanta [38]. As a result, "negative" flux quanta can be induced in the area between the dipoles without the quantization of flux quanta directly underneath the dipoles [37]. This contrasts previous studies in which positive and negative flux quanta emerge as vortex-antivortex pairs. In those experiments, the dipole size (> 1 μm) is larger than both the coherence length and penetration depth so the field is effectively screened prior to inducing flux quanta [33].

Conclusion

This study comprehensively examines the newfound dynamics between nanostructures in the magnetic vortex state and superconducting thin films. A hybrid system was constructed that allowed for the manipulation of its magnetic ordering, which in turn provided the ability to toggle the collective pinning of Abrikosov vortices in the superconductor. Previous studies have shown that inducing magnetic vortices in the nanodots can produce a bi-stable superconductivity in the film, but the control of the magnetic ordering and its interaction with a matching array of flux quanta is something unique to our experiments.

The suppressibility of vortex pinning in a superconductor by an external influence is an exciting effect and should continue to be investigated. Further analyzing the system's dependencies on temperature and thickness will give greater insight for the scalability and reproducibility of these structures. Further modification of the geometry may provide more drastic (or completely different) results and lend some understanding to the applicability of the effects we are witnessing. This research has only touched on a few of its many possible experimental variations, and future extensions of this project will offer a better conception of the underlying physics.

References

[1] O. Daldini, P. Martinoli, J.L. Olsen and G. Berner, Phys. Rev. Lett. **32**, 218 (1974).

[2] A.T. Fiory, A.F. Hebard and S. Somekh, Appl. Phys. Lett. **32**, 73 (1978).

[3] A. Pruymboom, P.H. Kes, E. van der Drift and S. Radelaar, Phys. Rev. Lett. **60**, 1430 (1988).

[4] Y. Otani, B. Pannetier, J.P. Noziers and D. Givord, J. Magn. Magn. Mater. **126**, 622 (1993).

[5] M. Baert, V.V. Metlushko, R. Jonckheere, V.V. Moshchalkov and Y. Bruynseraede, Phys. Rev. Lett. **74**, 3269 (1995).

[6] J.I. Martín, M. Velez, J. Nogues and I.K. Schuller, Phys. Rev. Lett. **79**, 1929 (1997).

[7] D.J. Morgan and J.B. Ketterson, Phys. Rev. Lett. **80**, 3614 (1998).

[8] M.J. Van Bael, J. Bekaert, K. Temst, L. Van Look, V.V. Moshchalkov, Y. Bruynseraede, G.D. Howells, A.N. Grigorenko, S.J. Bending and G. Borghs, Phys. Rev. Lett. **86**, 155 (2001).

[9] U. Welp, Z.L. Xiao, J.S. Jiang, V.K. Vlasko-Vlasov, S.D. Bader, G.W. Crabtree, J. Liang, H. Chik, and J.M. Xu , Phys. Rev. B **66**, 212507 (2002).

[10] M.I. Montero, J.J. Akerman, A. Varilci, and I.K. Schuller, Europhys. Lett. **63**, 118 (2003).

[11] J.E. Villegas , E.M. Gonzalez, Z. Sefrioui, J. Santamaria, and J.L. Vicent, Phys. Rev. B **72**, 174512 (2005).

[12] A.V. Silhanek, W. Gillijns, V.V. Moshchalkov, V. Metlushko, and B. Ilic , Appl. Phys. Lett. **89**, 182505 (2006).

[13] V. Misko, S. Savel'ev and F. Nori, Phys. Rev. Lett. **95**, 177007 (2005).

[14] J.E. Villegas, M.I. Montero, C.-P. Li and I.K. Schuller, Phys. Rev. Lett. **97**, 27002 (2006).

[15] M. Kemmler, C. Gürlich, A. Sterck, H. Pöhler, M. Neuhaus, M. Siegel, R. Kleiner and D. Koelle , Phys. Rev. Lett. **97**, 147003 (2006).

[16] A.I. Buzdin, Rev. Mod. Phys. **77**, 935 (2005).

[17] A. Palau, H. Parvaneh, N.A. Stelmashenko, H. Wang, J.L. Macmanus-Driscoll, and M.G. Blamire, Phys. Rev. Lett. **98**, 117003 (2007).

[18] G. Carneiro, Phys. Rev. B **69**, 214504 (2004).

[19] A. Libál, C. Reichhardt, C.J. Olson Reichhardt, Phys. Rev. Lett **97**, 228302 (2006).

[20] S. Tung, V. Schweikhard and E.A. Cornell, Phys. Rev. Lett. **97**, 240402 (2006).

[21] G. Grüner, Rev. Mod. Phys. **60**, 1129 (1988).

[22] T. Giamarchi and P. Le Doussal, Phys. Rev. Lett. **76**, 3408 (1996).

[23] R.P. Cowburn, D.K. Koltsov, A.O. Adeyeye, M.E. Welland, D.M. Tricker, Phys. Rev. Lett. **83**, 1042 (1999).

[24] T. Shinjo, T. Okuno, R. Hassdorf, K. Shigeto, T. Ono, Science **289**, 930 (2000).

[25] T. Okuno, K. Shigeto, T. Ono, K. Mibu and T. Shinjo, Jour. Mag. Mag, Mat. **240**, 1 (2002).

[26] H.F. Ding, A.K. Schmid, D. Li, K.Y. Guslienko, and S.D. Bader, Phys. Rev. Lett. **94**, 157202 (2005).

[27] R. K. Dumas, C.-P. Li, I.V. Roshchin, I.K. Schuller, and K. Liu, Phys. Rev. B **75**, 134405 (2007).

[28] J.E. Villegas, C.-P. Li and I.K. Schuller, Phys. Rev. Lett. in press (2007).

[29] C.P. Bean and J.D. Livingston, Phys. Rev. Lett. **12**, 14 (1964).

[30] V.V. Volkov and Y. Zhu, Microsc. Microanal. **11**, 1830 (2005).

[31] J.W. Lau, M. Beleggia, and Y. Zhu, Jour. Appl. Phys. **102**, 043906 (2007).

[32] M. Lange, M.J. Van Bael, Y. Bruynseraede, and V.V. Moshchalkov, Phys. Rev. Lett. **90**, 197006 (2003).

[33] W. Gillinjs, A.V. Silhanek and V.V. Moshchalkov, Phys. Rev. B **74**, 220509(R) (2006).

[34] J. Guimpel, F. de la Cruz, J. Murduck, and I.K. Schuller, Phys. Rev. B **35**, 3655 (1987).

[35] M. Lange, M.J. Van Bael, Y. Bruynseraede, and V.V. Moshchalkov, Phys. Rev.

Lett. **90**, 197006 (2003).

[36] M.V. Milosevic and F.M. Peeters, Phys. Rev. Lett. **93**, 267006 (2004).

[37] M.V. Milosevic and F.M. Peeters, Phys. Rev. B **68**, 024509 (2003).

[38] S. Kim, C.-R. Hu and M.J. Andrews, Phys. Rev. B **74**, 214511 (2006).